processes

MDPI

Article

Adaptive Drainage Pipe for Crystallization Prevention: Mechanism and Experimental Study

Zhen Liu [1], Xuefu Zhang [1], Shiyang Liu [1,*], Shaojie Guan [2], Weiyuan Tang [2] and Wei Meng [2]

[1] Institute of Future Civil Engineering Science and Technology, Chongqing Jiaotong University, Chongqing 400074, China
[2] College of Civil Engineering, Chongqing Jiaotong University, Chongqing 400074, China
* Correspondence: cqjtulsy@163.com

Abstract: Crystallization-induced blockages in tunnel drainage systems pose significant challenges to their functionality and longevity. To address this issue, this study proposes a novel adaptive drainage pipe designed to prevent crystallization. By constructing an indoor experimental model for anti-crystallization tests, combined with scanning electron microscopy (SEM) and molecular dynamics simulations, this study investigates the mechanism and effectiveness of the proposed system. The findings reveal that flexible PVC pipes in dynamic flow and expansion states significantly reduce crystallization compared to conventional PVC pipes. Among tested materials, EVA and TPU demonstrate superior crystallization resistance, with EVA exhibiting the lowest crystallization accumulation (7.13 g/m). Molecular dynamics simulations further elucidated the influence of material properties on the diffusion coefficient and binding energy of calcium carbonate crystals, with EVA showing the lowest binding energy with calcium carbonate at 135.11 kcal/mol, ultimately confirming EVA as the optimal material for crystallization prevention. These results offer new strategies and valuable references for managing crystallization in tunnel drainage systems.

Keywords: tunnel engineering; adaptive drainage pipe; calcium carbonate crystallization; diffusion coefficient; molecular dynamics

Received: 28 November 2024
Revised: 9 January 2025
Accepted: 10 January 2025
Published: 14 January 2025

Citation: Liu, Z.; Zhang, X.; Liu, S.; Guan, S.; Tang, W.; Meng, W. Adaptive Drainage Pipe for Crystallization Prevention: Mechanism and Experimental Study. *Processes* **2025**, *13*, 214. https://doi.org/10.3390/pr13010214

1. Introduction

During tunnel operation, crystallization within drainage pipes often leads to blockages, potentially causing the failure of the drainage system. Addressing this issue has emerged as a critical area of research in tunnel engineering.

In terms of crystallization influencing factors, an increasing number of studies and publications have focused on the widespread formation of $CaCO_3$ scale deposits in tunnel drainage systems [1–4]. Most scale deposits primarily consist of calcite, with minor amounts of aragonite and/or vaterite also present [5]. The deposition of $CaCO_3$ is typically influenced by the following factors: (i) CO_2 exchange between the tunnel (or drainage system) atmosphere and the discharged water solution, (ii) the mixing of solutions with different compositions, (iii) microbial activity, and/or (iv) site-specific fluid–solid interactions (e.g., dissolution of carbonate host rocks and/or cementitious materials such as portlandite ($Ca(OH)_2$)) [6,7]. The geometry of the tunnel, as well as the concentrations of Ca^{2+} and CO_3^{2-} in the interacting groundwater or fissure solutions, generally determine the intensity of $CaCO_3$ scale formation [8,9]. By constructing hydrochemical models that take into account environmental factors, operating conditions, and anthropogenic influences, the mechanisms of scale deposit formation can be assessed and quantified [6].

In terms of prevention and mitigation, several studies have explored techniques for preventing crystallization in drainage pipes. Qu [10] and Zhou [11] analyzed karst tunnel drainage systems in central and western China, identifying key factors and patterns contributing to crystallization. They proposed preventive measures such as installing specialized pipes at critical locations and introducing high-efficiency scale inhibitors to mitigate crystallization blockages. Zhuge [12] et al. observed, through extensive experimental studies, that linear material bundles form during the early stages of ultrafine calcium carbonate crystallization. Drawing on the principles of biomineralization, Zhu [13] et al. introduced lignin as an organic matrix in the calcium carbonate growth process. Their research demonstrated that lignin concentration and growth temperature significantly influence the crystallization process, resulting predominantly in calcite-shaped calcium carbonate crystals. Parsons et al. [14] posited that magnetic fields accelerate ion interactions in solutions, promoting rapid crystal formation. Coey [15] further demonstrated through experiments that magnetic fields encourage calcium carbonate crystals to transform into aragonite or vaterite, which, due to their lower density compared to calcite, are more easily flushed away, effectively achieving descaling. Advanced methods combining molecular dynamics simulations and scanning electron microscopy have also been employed to investigate the effects of organic acids and scale inhibitors on calcium carbonate dissolution and crystallization mechanisms. Certain organic acids exhibit dual functionality, dissolving calcium carbonate while acting as scale inhibitors [16–23]. Techniques such as applying high-pressure electrostatic fields [24–26] or magnetic fields [27] alter the motion and crystallization behavior of ions in water, achieving anti-scaling effects. Furthermore, flocked drainage pipes have been shown to maintain stable crystallization levels, as the fabric pile exhibits lower binding energy with crystalline structures [28,29]. This unique property enables flocked drainage pipes to modify fluid flow fields, reducing crystallization.

Despite advances in crystallization prevention, current technologies primarily focus on optimizing the design and structure of existing pipes. However, research on reducing crystallization adhesion through pipe deformation remains limited. To address this gap, this study introduces an innovative adaptive drainage pipe design to prevent crystallization. Laboratory experiments, microscopic analyses, and molecular dynamics simulations are employed to elucidate the effects of various materials on calcium carbonate crystallization adhesion. By delving into the underlying mechanisms through molecular simulations, this research offers novel insights and strategies for preventing crystallization in tunnel drainage systems.

2. Mechanism Analysis of Adaptive Drainage Pipes for Crystallization Prevention

2.1. Dynamic Flow Mechanism (Biomimetic Intestinal Peristalsis)

Inspired by the natural peristaltic motion of the human intestine, the adaptive design integrates a flexible inner pipe housed within a rigid plastic outer pipe. As water flows through the inner flexible pipe, it induces rhythmic, wave-like contractions and expansions that mimic intestinal peristalsis. This dynamic motion not only facilitates the flow of water but also disrupts the adhesion of calcium carbonate crystals to the inner walls of the pipe. By continuously agitating the inner surface, the system significantly reduces crystallization compared to static or rigid pipe designs. This biomimetic approach leverages the self-cleaning behavior of biological systems, effectively preventing the buildup of scaling and ensuring longer operational efficiency for water transport systems.

2.2. Expansion-Induced Crystallization Detachment (Biomimetic Intestinal Expansion)

Taking inspiration from the intestinal dilation mechanism during digestion, the design incorporates an expansion-based cleaning strategy. In situations where minor crystallization has formed on the inner walls of the flexible pipe, episodes of high water flow—such as during the rainy season—trigger the pipe to undergo significant expansion and elongation. This behavior mirrors the expansion of intestinal walls during the passage of food or gas. The mechanical force generated during this expansion exerts stress on the adhered calcium carbonate crystals, causing them to fracture and dislodge. The dislodged particles are subsequently flushed out by the increased water flow, restoring the inner surface of the pipe to its clean state. This biomimetic feature ensures that the system can adaptively manage crystallization, even under variable water flow conditions, reducing maintenance needs and enhancing reliability. By adopting principles from the self-maintaining mechanisms of biological systems, this design demonstrates how biomimicry can lead to innovative and sustainable engineering solutions for scaling-related challenges in fluid transport systems.

2.3. Water Retention Mechanism for Crystallization Prevention

The flexible pipe's elasticity enables it to retain small amounts of water during dry seasons when water flow is minimal or absent. Under typical environmental exposure, calcium carbonate tends to harden over time. However, the retained water within the flexible pipe prevents the crystals from drying and hardening, instead keeping them soft and viscous. When the next rainy season brings increased water flow, these softened deposits are easily washed away.

3. Indoor Experiment Design and Test Methods

3.1. Experimental Materials and Apparatus

Analysis of existing drainage pipes and crystallization patterns reveals that different hydrophobic materials exhibit varying interactions with calcium carbonate crystals. High-performance hydrophobic materials can effectively prevent crystal adhesion, serving as a preventive measure. This study investigates the interaction between various hydrophobic materials and calcium carbonate crystals, as well as the peristaltic properties of flexible pipes.

The experiment utilized deionized water produced by a purifier, mixed with 4.5 kg of analytical-grade calcium carbonate powder and 0.5 kg of 80-mesh calcite. This setup allows observation of calcium carbonate's contact, adhesion, and accumulation on different materials. Since calcium carbonate is insoluble and prone to rapid precipitation, continuous stirring was employed to maintain its flow throughout the water circulation process.

The experimental setup featured a novel design: a 50 mm flexible pipe placed inside a 75 mm rigid pipe. The flexible pipe was secured at four points—both ends and the middle—while maintaining appropriate looseness to allow flexibility, as shown in Figure 1a. A custom-built circulation system was employed (Figure 1b) to simulate the accumulation and crystallization of calcium carbonate in tunnel drainage pipes.

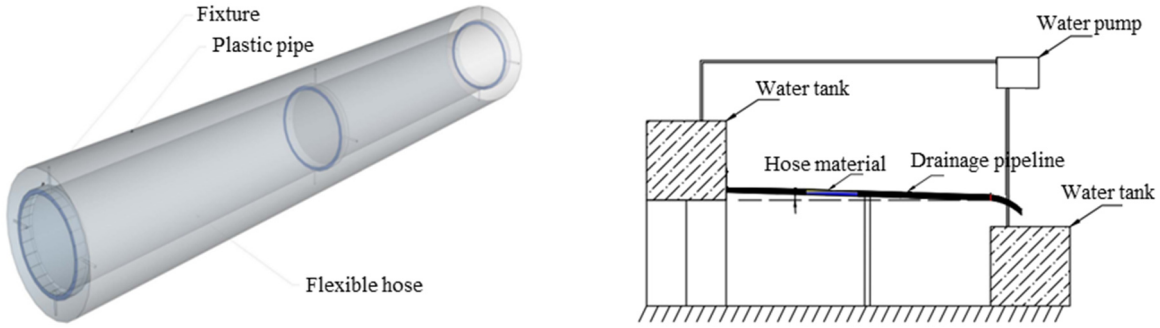

(**a**) (**b**)

Figure 1. Schematic diagram of experimental pipe (**a**) and schematic diagram of model (**b**).

3.2. Experimental Plan

The experiment involved three types of thin films (PVC, EVA, and TPU), with a raw PVC pipe serving as the control group. Each material underwent triplicate testing to ensure reproducibility. The water level in the upper tank was maintained at a constant height of 20 cm to ensure consistent flow velocity at the pipe inlet. The length of each pipe segment was set to 1 m.

Crystallization within the pipes was observed and measured over time using a 7-day cycle: 5 days of water circulation followed by 2 days of air drying, after which the mass of crystallized material was recorded. The average results from the three tests for each material were compared to analyze the crystallization tendencies. The experimental conditions are summarized in Table 1.

Table 1. Test conditions for different film materials in pipes.

Pipe Material	First Group	Second Group	Third Group
TPU	1.1	2.1	3.1
EVA	1.2	2.2	3.2
PVC	1.3	2.3	3.3
Raw PVC pipe control	1.4	2.4	3.4

Note: The numbers in the table represent the working condition codes.

3.3. Test Methods

3.3.1. Weight Weighing Method

In this study, the indoor tests were conducted in an open indoor environment, with each cycle lasting 7 days, and a total of 7 cycles were performed. To minimize experimental errors, the drainage pipes were weighed three times at the end of each cycle, and the average value was used to calculate the crystallization increment. Furthermore, to reduce errors between experimental groups, three parallel tests were conducted for each drainage pipe, and the average crystallization increment for each group was calculated. The final crystallization increment was determined by averaging these group averages.

3.3.2. SEM Test

After the experiment, the crystallized section of the pipe was cut into small samples measuring 5 mm × 5 mm × 3 mm. Subsequently, the samples were dried in a vacuum drying oven at 60 °C for 24 h. Finally, gold sputter coating was applied to the samples, and scanning electron microscopy (SEM) analysis was performed using a Zeiss Sigma300 thermal field emission scanning electron microscope (Carl Zeiss AG, Oberkochen, Germany) at an accelerating voltage of either 2 kV or 3 kV.

3.3.3. Model Construction

The process of constructing models using Materials Studio involved the following steps: (1) Initially, polymer monomers or repeating units of EVA, TPU, and PVC materials were constructed. (2) Based on the density of each material, models of EVA, TPU, and PVC polymer films were created. (3) Additionally, a calcium carbonate (CaCO3) solution model was established, and solid–liquid composite models of EVA-CaCO3, TPU-CaCO3, and PVC-CaCO3 were developed. The models were further validated according to the material densities. For detailed modeling procedures and parameters, please refer to Section 5.1.

4. Experimental Results and Discussion

4.1. Performance Comparison of Flexible and Raw Pipes with the Same PVC Material

4.1.1. Evaluation of Crystallization Resistance and Growth Patterns

To minimize experimental error and enhance the rigor and accuracy of the analysis, three replicate tests were conducted. The crystallization resistance of different materials was assessed using the dry weight per meter as a standardized metric. The evaluation formula is as follows:

$$m_t = \frac{m}{l}$$

where

m_t is the dry weight per meter of the pipe section in the t-th cycle (g/m).
m is the total dry weight of crystallization in the pipe section (g).
l is the length of the pipe section (m).

To analyze the crystallization growth patterns across cycles, the cumulative crystallization amount for each test was calculated using the following formula:

$$\Delta m_t = m_t - m_0$$

where

Δm_t is the cumulative crystallization amount per meter for the t-th cycle (g/m).
m_t is the dry weight per meter of the pipe section for the t-th cycle (g/m).
m_0 is the initial dry weight per meter of the raw pipe section (g).

4.1.2. Statistical Analysis of Experimental Results

As shown in Figure 2, crystallization growth remained relatively low, with the PVC film pipe exhibiting an increase of 1.25 g/m and the raw PVC pipe showing 1.30 g/m. However, during the mid-phase, crystallization increased noticeably. The PVC flexible pipe reached a peak growth of 1.36 g/m in the third cycle, while the raw PVC pipe peaked at 1.39 g/m in the second cycle. This trend is attributed to the difficulty of initial crystallization adhesion. Once a base layer of crystallization forms, subsequent crystals adhere more readily to the calcium carbonate deposits, resulting in rapid growth. Following the peak, the crystallization amount decreased and gradually stabilized.

As shown in Figure 3, the total cumulative crystallization on the PVC flexible pipe was 8.54 g/m, compared to 9.27 g/m for the raw PVC pipe. This highlights the superior crystallization resistance of the flexible pipe, attributed to its dynamic behavior under the impact of water flow. The flexible pipe film undergoes a creeping motion, maintaining a dynamic state that contrasts sharply with the static nature of the rigid plastic pipe. This dynamic state effectively reduces crystallization adhesion on the flexible pipe, enhancing its resistance to crystallization formation and growth.

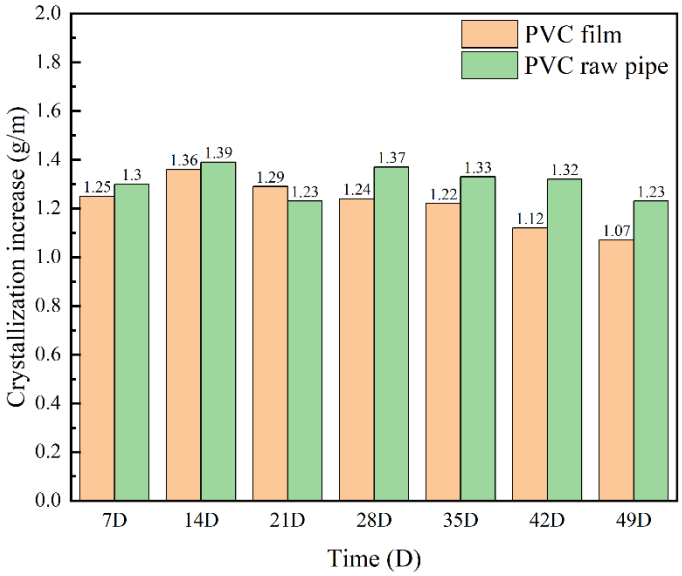

Figure 2. Crystallization growth of PVC flexible and raw pipes.

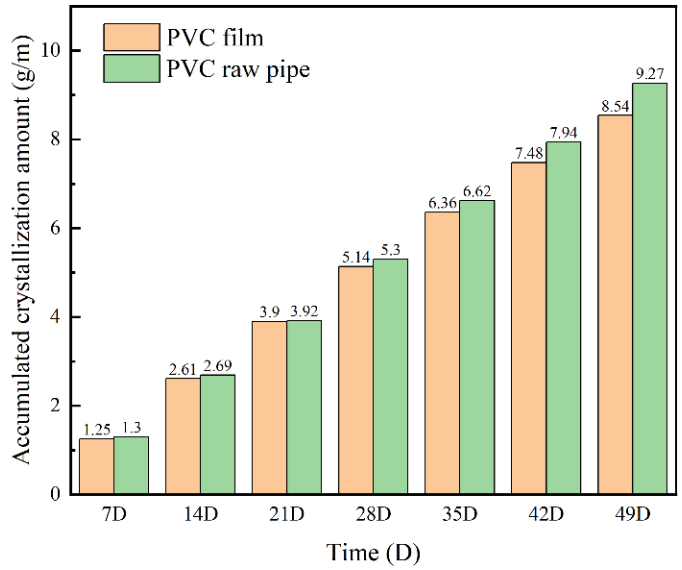

Figure 3. Cumulative crystallization of PVC flexible and raw pipes.

4.2. Performance of Flexible Pipes with Different Materials

4.2.1. TPU and EVA Film Pipes

Three types of flexible film pipes—EVA, TPU, and PVC—were compared under identical conditions to evaluate their crystallization resistance.

As shown in Figure 4, EVA exhibited an initial crystallization of 0.98 g/m in the first cycle, reaching a maximum of 1.14 g/m in the fourth cycle. TPU began at 1.04 g/m in the first cycle, peaking at 1.22 g/m in the second cycle. During the early stages, crystal adhesion to the film surface was difficult. However, once initial adhesion occurred, subsequent crystallization became easier. As crystallization progressed, partial detachment of crystals prevented excessive growth.

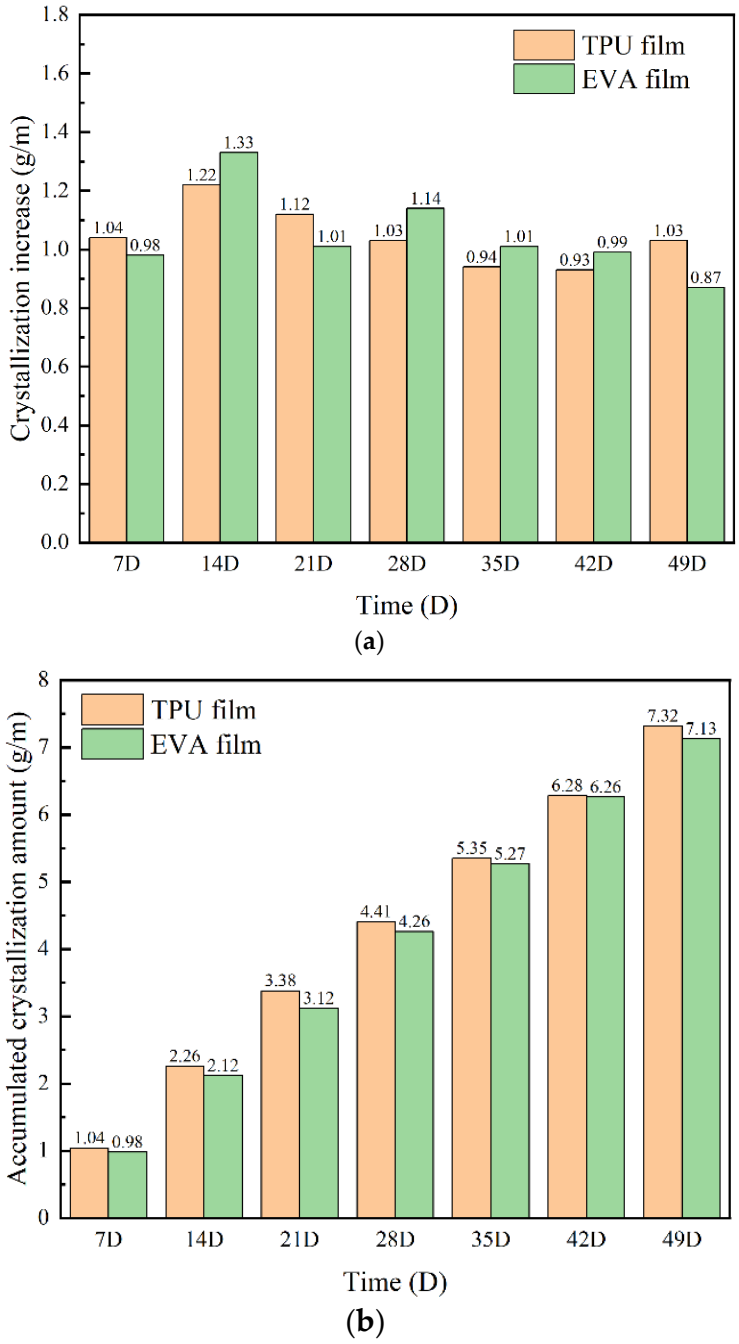

Figure 4. Stage-wise crystallization in TPU and EVA film pipes. (**a**) Cumulative crystallization growth in TPU and EVA film pipes. (**b**) Stage-wise cumulative crystallization in TPU and EVA film pipes.

4.2.2. Comparison of Film Pipes and Raw PVC Pipe

Cumulative crystallization levels were analyzed across all pipe types. As depicted in Figure 5, EVA demonstrated the best crystallization resistance, with a final cumulative crystallization of only 7.13 g/m. TPU followed closely at 7.32 g/m. In contrast, the PVC film pipe and raw PVC pipe showed significantly higher cumulative crystallization levels of 8.51 g/m and 9.27 g/m, respectively.

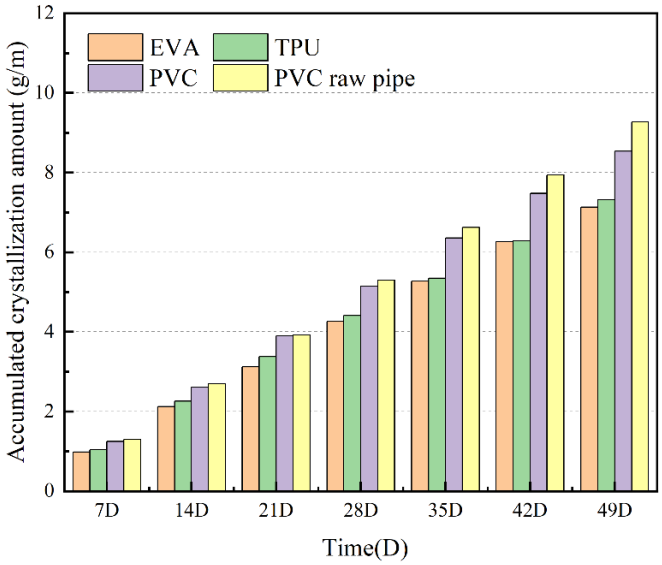

Figure 5. Increase in cumulative crystallization in pipes of different materials.

4.3. SEM (Scanning Electron Microscopy) Analysis of Crystalline Deposits

To further investigate the composition and microscopic characteristics of crystalline deposits, samples were extracted from the surfaces of various film pipes and raw PCV pipe for SEM analysis. This allowed for a detailed examination of the microstructure, including grain size, shape, and crystal configuration.

As illustrated in Figure 6, both EVA and TPU exhibited significant cracking in the attached crystals, while the PVC film pipe displayed only minor cracking. In contrast, no cracks were observed on the raw PVC pipe. These findings suggest that the elasticity and flexibility of EVA and TPU materials cause cracks and detachment in adhered crystals, improving crystallization resistance. PVC film pipes, being relatively rigid, exhibited less cracking. The rigid raw PVC pipe showed no evidence of cracking, reflecting its static nature.

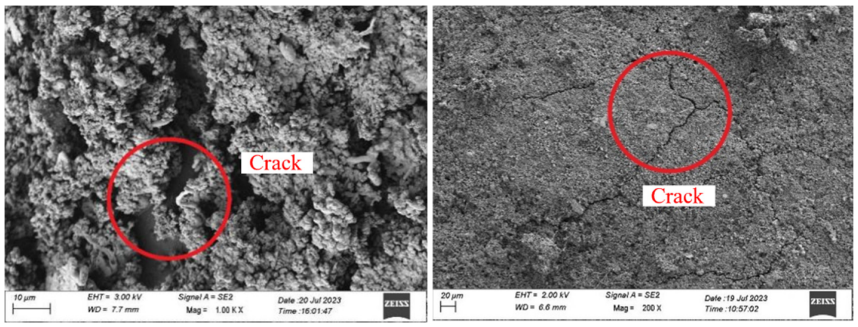

(**a**) SEM of EVA

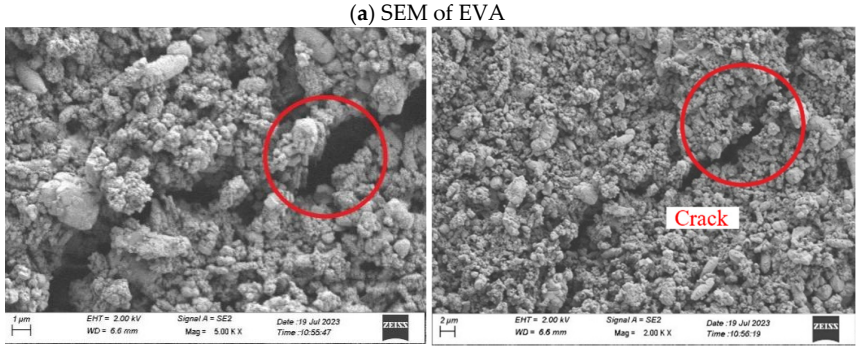

(**b**) SEM of TPU

Figure 6. *Cont.*

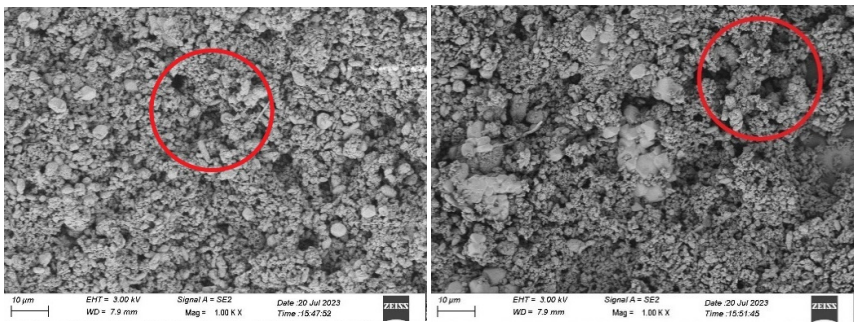

(**c**) SEM of PVC film

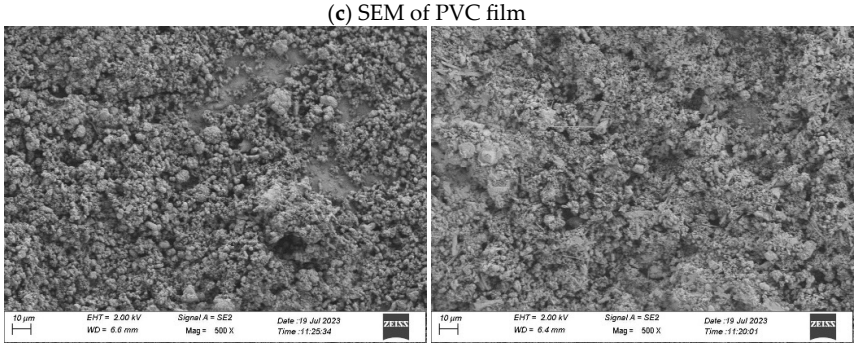

(**d**) SEM of raw PVC pipe

Figure 6. SEM images of crystalline deposits.

5. Analysis of the Crystallization Prevention Mechanism in Adaptive Drainage Pipe Materials

5.1. Molecular Model Construction and Simulation Details

The specific steps for constructing models using Materials Studio are as follows: First, monomers of EVA (composed of ethylene and vinyl acetate), TPU (crosslinked by diisocyanate and polyether), and PVC were constructed. Based on these monomers, polymers with a degree of polymerization of 10 were created, and thin-film models of EVA, TPU, and PVC were developed using 20 polymer chains. For each thin-film model, simulations were performed under the NPT ensemble with a temperature of 300 K, a pressure of 0 GPa, a time step of 1 fs, and a simulation duration of 100 ps. The density values obtained from the models fell within the range of actual densities, indicating the rationality of the models. Additionally, a solution model containing 4 Ca^{2+}, 6 Na^{+}, 7 CO_3^{2-}, and 800 water molecules was constructed, and solid–liquid composite models of EVA-$CaCO_3$ (Figure 7a), TPU-$CaCO_3$ (Figure 7b), and PVC-$CaCO_3$ (Figure 7c) were further developed. Specific parameters are provided in Table 2. It is worth noting that the actual membrane materials are doped with other substances, while the simulated models focus primarily on the main components. As a result, there are certain differences between the simulated models and the actual membrane materials.

After constructing the model boxes, the CVFF force field was selected for geometric optimization. Through this optimization process, structural energy gradually converged, ultimately yielding stable energy composite models. Subsequently, dynamic simulations were performed to calculate the diffusion coefficients of H_2O, Ca^{2+}, and CO_3^{2-} within the calcium carbonate solution, as well as the binding energies between the polymers and the solution. The specific simulation parameters are detailed in Table 3.

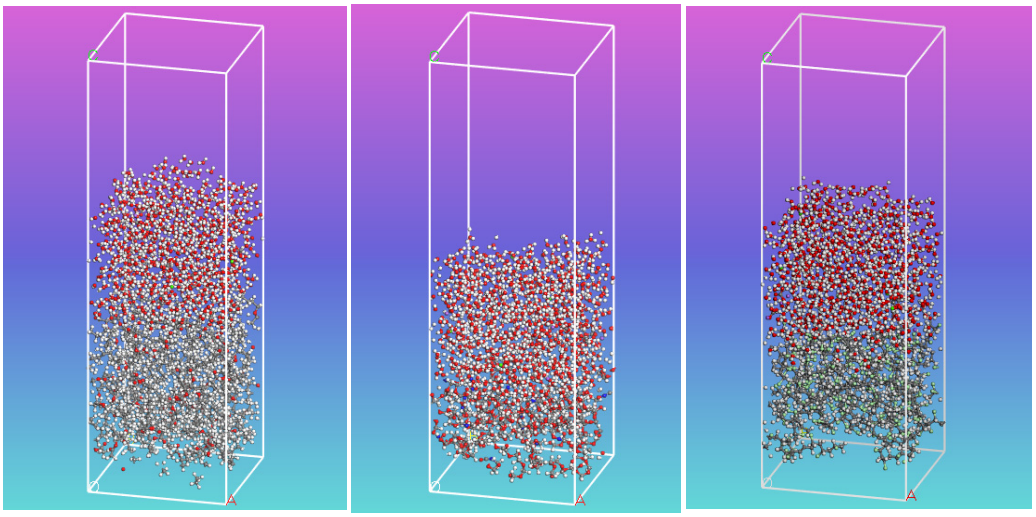

(**a**) (**b**) (**c**)

Figure 7. Molecular dynamics simulation models: (**a**) EVA-$CaCO_3$ model; (**b**) TPU-$CaCO_3$ model; (**c**) PVC-$CaCO_3$ model. Red represents oxygen atoms, gray represents carbon atoms, light green represents calcium atoms, white represents hydrogen atoms, purple represents nitrogen atoms, and pale green represents chlorine atoms.

Table 2. Model parameters.

	EVA	TPU	PVC
Degree of polymerization	10	10	10
Number of monomers	20	20	20
Ensemble	NPT	NPT	NPT
Temperature (K)	300	300	300
Pressure (GPa)	0	0	0
Simulate density (g/cm^3)	0.932	1.21	1.38
Actual density (g/cm^3)	0.93–0.95	1.1–1.25	1.35–1.45

Table 3. Basic computational parameters.

Computational Parameters	Parameter Values
Ensemble	NVT
Temperature Control	Andersen
Temperature Range	300 K
Time Step	1.00 fs
Computation Time	200 ps

5.2. Molecular Dynamics Simulation Results and Discussion

5.2.1. Temperature and Energy Stability Analysis

Simulation calculations were conducted using the Forcite module under a canonical ensemble (NVT). Initially, the Velocity Scale method was used for temperature control to ensure equilibrium. A subsequent dynamic calculation utilized the Andersen thermostat under identical conditions. During the second phase, temperature fluctuations remained minimal, confirming the system's equilibrium state. Analysis was performed on data from this stabilized phase.

The initial model temperature was set to 298 K. After 200 ps of computation, the temperature stabilized within ±10% of the set value. This consistency, combined with the energy output's minimal fluctuations, demonstrated that the system had achieved a stable and optimal state for molecular dynamics simulations.

5.2.2. Diffusion Coefficient Analysis

In molecular dynamics systems, atomic positions change continuously. At any given moment time t, a particle's position r_t is defined. The mean square displacement (MSD) and diffusion coefficient D can be expressed as follows:

$$MSD = R_t = \left\langle \left| \vec{\gamma_t} - \vec{\gamma_0} \right|^2 \right\rangle$$

where

R_t is the mean square displacement,

<> denotes the average.

$$\lim_{t \to \infty} \left\langle \left| \vec{\gamma_t} - \vec{\gamma_0} \right|^2 \right\rangle = 6D_t$$

where

D is the diffusion coefficient.

The diffusion coefficient quantifies molecular or ionic mobility, with higher values indicating greater activity and reduced likelihood of interaction. Analyzing diffusion coefficients for key components such as H_2O, Ca^{2+}, and CO_3^{2-} offers insights into the crystallization patterns observed in macroscopic phenomena (Figure 8).

The MSD fitting curves in Figure 8 show R^2 values greater than 0.9, indicating high accuracy. Consequently, the diffusion coefficient calculations advance the analysis of how different materials affect crystallization patterns. Table 4 reveals that the diffusion coefficients for Ca^{2+} and CO_3^{2-} are similar, thus the H_2O diffusion coefficient will serve as a benchmark to analyze its influence on Ca^{2+} and CO_3^{2-}. The ratios in Table 5 offer a clearer comparison.

Table 4. Diffusion coefficients for H_2O, Ca^{2+}, and CO_3^{2-} in various materials.

Pipe Material	H_2O Diffusion Coefficient/(10^{-5})	Ca^{2+} Diffusion Coefficient/(10^{-5})	CO_3^{2-} Diffusion Coefficient/(10^{-5})
EVA	3.0485	0.7180	0.7010
TPU	5.1040	1.5267	1.5273
PVC	4.4098	1.6115	1.4027

Table 5. Ratio multiple of the diffusion coefficient of H_2O.

Pipe Material	Ratios Relative to H_2O Diffusion Coefficients		
EVA	1.00	4.2458	4.3488
TPU	1.00	3.3432	3.3418
PVC	1.00	2.7365	3.1439

Based on Table 4, EVA exhibited the largest diffusion ratio for H_2O compared to Ca^{2+} and CO_3^{2-}, at over 4:1. This indicates significant H_2O mobility in EVA solutions, restricting Ca^{2+} and CO_3^{2-} movement and thus limiting $CaCO_3$ crystallization. TPU showed a ratio exceeding 3:1, while PVC's ratio was above 2:1. Consequently, EVA minimizes crystallization most effectively, followed by TPU, with PVC allowing the highest crystallization.

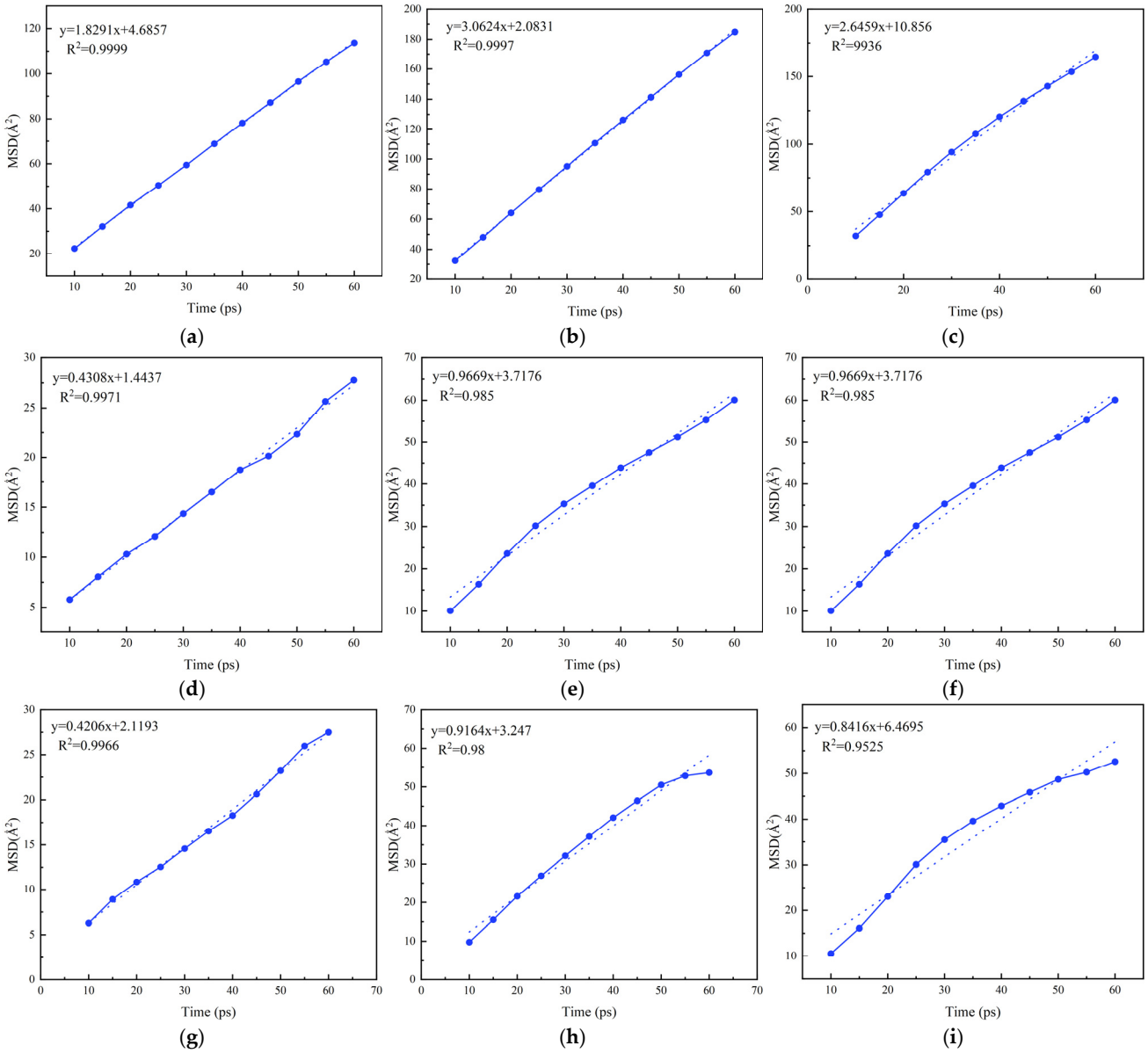

Figure 8. Fitted mean square displacement curves: (**a**–**c**) for H_2O in EVA, TPU, and PVC, (**d**–**f**) for Ca^{2+} in EVA, TPU, and PVC, (**g**–**i**) for CO_3^{2-} in EVA, TPU, and PVC.

5.2.3. Binding Energy Analysis

The interaction between Ca^{2+}, CO_3^{2-}, EVA, TPU, PVC, and the calcium carbonate crystal plane is reflected in the binding energy. A stronger interaction indicates a higher likelihood of the ions adhering to the crystal plane and forming new crystals. By calculating the binding energy, the adhesive capacity of the crystalline structure can be assessed, enabling a comparative analysis of adhesion across different materials. The formula for binding energy is as follows:

$$\Delta E = E_{total} - \left(E_{surface} + E_l\right)$$

$$E_{binding} = -\Delta E$$

where

$E_{binding}$ —Binding energy (kcal/mol),

E_{total} —Total energy of the crystal plane and solution system (kcal/mol),

$E_{surface}$ —Single-point energy of the crystal plane (kcal/mol),
E_l—Energy of the solution system (kcal/mol).

Lower binding energies signify weaker adhesion and reduced crystallization. Table 6 compares the adhesion and binding energy for the crystallization of calcium carbonate with EVA, TPU, and PVC. Among these materials, EVA exhibits the lowest binding energy at 135.11 kcal/mol, followed by TPU at 242.82 kcal/mol, and PVC at 403.13 kcal/mol. The binding energy sequence, EVA < TPU < PVC, aligns with diffusion coefficient results, confirming EVA's superior crystallization resistance.

Table 6. Binding energy comparison across different materials.

Pipe Material	E_{total} kcal/mol	E_{surfac} kcal/mol	E_l kcal/mol	ΔE kcal/mol	$E_{binding}$ kcal/mol
EVA	−14,335.7	−1250.98	−12,949.6	−135.106	135.1056
TPU	−14,162.7	−750.587	−13,169.3	−242.817	242.8174
PVC	−15,117.6	−1974.5	−12,739.9	−403.129	403.1292

6. Discussion

This study, through experiments and molecular dynamics simulations, revealed the mechanisms by which flexible drainage pipes and their materials prevent calcium carbonate crystallization at multiple levels. The results demonstrate that the design of flexible drainage pipes combines two biomimetic mechanisms: dynamic flow and expansion-induced crystallization detachment, significantly reducing crystal adhesion and accumulation on the pipe walls. This design mimics intestinal peristalsis and expansion behaviors, enabling easier detachment of crystals through dynamic disturbance and periodic deformation, thereby inhibiting the stable adhesion of initial crystals. This mechanism aligns with the findings of Mangestiyono et al. [30,31], who reported that vibration effectively reduces scaling, further validating the advantages of flexible designs for crystallization prevention.

EVA material exhibited the lowest crystallization accumulation, a performance attributed to its high diffusion coefficient and low binding energy. Molecular dynamics simulations revealed that the water diffusion coefficient of EVA is over four times greater than that of Ca^{2+} and CO_3^{2-}, with the high diffusion ratio enhancing solution fluidity and reducing ion aggregation. Additionally, its binding energy is the lowest (135.11 kcal/mol), significantly weakening the adhesion force between crystals and the pipe walls, making the crystals easier to detach. In contrast, TPU and PVC showed poorer anti-crystallization performance due to their lower diffusion ratio and higher binding energy.

SEM analysis provided micro-level evidence to support these findings. Crystals on the surfaces of EVA and TPU materials exhibited noticeable cracks, while such phenomena were not observed on PVC and rigid PVC pipes. This indicates that the elastic properties of flexible materials can disrupt the stability of crystals under mechanical force, enhancing the rate of crystallization detachment. The dynamic movement of flexible pipes further amplified this effect, especially under high flow conditions (e.g., during rainy seasons), where pipe expansion caused the crystallization layer to fracture and detach more easily. This mechanism aligns with previous studies [32–35], demonstrating the critical role of dynamic deformation on material surfaces in crystal adhesion and detachment.

Molecular dynamics simulations further deepened the understanding of the relationship between molecular structure and crystallization behavior. The ethylene-vinyl acetate structure of EVA demonstrated significant water molecule diffusivity, likely due to its non-polar groups reducing the hydrogen bond network density among water molecules, thereby enhancing solution fluidity. In contrast, the molecular structures of TPU and PVC restricted water molecule mobility and increased the local concentration of Ca^{2+} and CO_3^{2-},

facilitating crystal formation. Additionally, binding energy analysis showed that EVA's low binding energy effectively weakened the adhesion between crystals and pipe walls, while TPU and PVC, with higher binding energies, made crystals more resistant to detachment by fluid forces. These findings are consistent with previous research on how magnetic and electric fields alter crystal adhesion properties [36–39].

This study not only provides scientific evidence for the effectiveness of dynamic flexible pipe designs but also highlights the superior performance of EVA material in preventing crystallization. These findings offer important directions for the development and optimization of materials in the future, such as improving anti-crystallization performance by adjusting material molecular structures, including increasing flexible chain segments or reducing polar groups.

7. Conclusions

This study conducted an in-depth analysis of the performance and crystallization-preventing mechanisms of a novel adaptive drainage pipe through a combination of indoor experiments, SEM microtests, and molecular dynamics simulations. The main conclusions are as follows:

- A comparative analysis of flexible and raw PCV pipes made from the same PVC revealed a distinct crystallization growth pattern, initially increasing, then decreasing, and finally stabilizing. The total cumulative crystallization for the PVC flexible pipes was 8.54 g/m, compared to 9.27 g/m for the PVC raw pipes. Detailed experimental analysis and calculations confirmed that the PVC flexible pipes outperformed the raw PVC pipes in terms of crystallization prevention.
- Among various flexible materials, EVA flexible pipes displayed significant superiority in preventing crystallization. In the final experimental data, the cumulative crystallization amount for EVA flexible pipes was only 7.13 g/m, followed by TPU film material at 7.32 g/m. In comparison, the PVC film pipes and raw PVC pipes had cumulative crystallization amounts of 8.51 g/m and 9.27 g/m, respectively, both exceeding those of EVA and TPU.
- Molecular dynamics revealed the relationship between the diffusion coefficients of H_2O, Ca^{2+}, and $CO_3{}^{2-}$ in calcium carbonate solutions within different pipes and their impact on calcium carbonate crystallization. In EVA materials, the diffusion coefficient of H_2O was more than four times that of Ca^{2+} and $CO_3{}^{2-}$, resulting in the least influence on calcium carbonate crystallization. TPU and PVC materials exhibited smaller effects, with H_2O being over three times that of Ca^{2+} and $CO_3{}^{2-}$ in TPU, and twice as much in PVC, leading to higher crystallization amounts.
- Among the three materials, EVA exhibited the lowest binding energy with calcium carbonate at 135.11 kcal/mol, followed by TPU at 242.82 kcal/mol, and PVC at 403.13 kcal/mol. A comprehensive analysis of the binding energy and the crystallization trends observed in indoor experiments confirmed the consistency between experimental and simulation results. EVA material showed the least crystallization, indicating superior performance, followed by TPU, while PVC exhibited the poorest crystallization prevention.

Author Contributions: Conceptualization, Z.L. and S.L.; Methodology, Z.L.; Software, Z.L. and W.T.; Validation, S.L. and W.T.; Formal analysis, Z.L.; Resources, X.Z.; Data curation, S.L.; Writing—original draft, Z.L.; Writing—review & editing, Z.L., X.Z., S.L., S.G., W.T. and W.M.; Supervision, X.Z. and S.L.; Project administration, X.Z.; Funding acquisition, X.Z. All authors have read and agreed to the published version of the manuscript.

Funding: This research was financially supported by the Science and Technology Research Program of Chongqing Municipal Education Commission (Grant No. KJQN202400748), the cooperation between Chongqing University and the Institute of Chinese Academy of Sciences (No. HZ2021009), the Chongqing Talent Innovation and Entrepreneurship Leading Talent Project (CQYC202203091118), and the Chongqing Municipal Talent Plan "Contract System" Project Plan (cstc2024ycjh-bgzxm0219).

Data Availability Statement: Data is contained within the article.

Conflicts of Interest: The authors declare that there are no conflicts of interest.

References

1. Rinder, T.; Dietzel, M.; Leis, A. Calcium carbonate scaling under alkaline conditions–case studies and hydrochemical modelling. *Appl. Geochem.* **2013**, *35*, 132–141. [CrossRef]
2. Jia, N.; Tassin, B.; Calon, N.; Deneele, D.; Koscielny, M.; Prévot, F. Scaling in railway infrastructural drainage devices: Site study. *Innov. Infrastruct. Solut.* **2016**, *1*, 42. [CrossRef]
3. Xin, Z.; Moon, J.H.; Kim, Y.U. Reduction of adherent forces of sedimentous contaminants in tunnel drainage using vibrations from flexible and transparent organic films. *KSCE J. Civ. Eng.* **2018**, *22*, 2619–2622. [CrossRef]
4. Chen, Y.; Cui, Y.; Barrett, A.G.; Chille, F.; Lassalle, S. Investigation of calcite precipitation in the drainage system of railway tunnels. *Tunn. Undergr. Space Technol.* **2019**, *84*, 45–55. [CrossRef]
5. Zhang, X.; Zhou, Y.; Zhang, B.; Zhou, Y.; Liu, S. Investigation and Analysis on Crystallizat ion of Tunnel Drainage Pipe in Chongqing. *Adv. Mater. Sci. Eng.* **2018**, *18*, 1–6.
6. Eichinger, S.; Boch, R.; Leis, A.; Koraimann, G.; Grengg, C.; Domberger, G.; Nachtnebel, M.; Schwab, C.; Dietzel, M. Scale deposits in tunnel drainage systems–A study on fabrics and formation mechanisms. *Sci. Total Environ.* **2020**, *718*, 137140. [CrossRef]
7. Boch, R.; Dietzel, M.; Reichl, P.; Leis, A.; Baldermann, A.; Mittermayr, F.; Pölt, P. Rapid ikaite ($CaCO_3 \cdot 6H_2O$) crystallization in a man-made river bed: Hydrogeochemical monitoring of a rarely documented mineral formation. *Appl. Geochem.* **2015**, *63*, 366–379. [CrossRef]
8. Dietzel, M.; Rinder, T.; Niedermayr, A.; Mittermayr, F.; Leis, A.; Klammer, D.; Köhler, S.; Reichl, P. Ursachen und Mechanismen der Versinterung von Tunneldrainagen. *BHM Berg-Und Hüttenmännische Monatshefte* **2008**, *153*, 369–372. [CrossRef]
9. Girmscheid, G.; Gamisch, T.; Klein, T.; Meinlschmidt, A. Versinterung von Tunneldrainagen-Mechanismen Der Versinterungsentstehung. *Bauingenieur* **2003**, *78*, 292–300.
10. Qu, M. Study on the Crystallization Blockage Law of Tunnel Drainage System in Limestone Area. Master's Thesis, Chongqing Jiaotong University, Chongqing, China, 2016.
11. Zhou, Z. Research on the Mechanism of Groundwater Seepage Crystallization Blocking Tunnel Drainage Pipes in Karst Areas and Treatment Suggestions. Master's Thesis, Changan University, Xi'an, China, 2015.
12. Zhuge, L.; Zhang, S.; Han, Y.; Jiang, J. Crystallization process of ultrafine calcium carbonate and synthesis of ultrafine calcium carbonate with different morphologies. *Chem. Res.* **1998**, *03*, 26–30.
13. Zhu, W.; Luo, X.; He, P.; Lu, Y. The effect of lignin on the crystallization behavior of calcium carbonate. *Chem. Ind. For. Prod.* **2010**, *06*, 7–12.
14. Parsons, S.A.; Wang, B.L.; Judd, S.J.; Stephenson, T. Magnetic treatment of calcium carbonate scale—Effect of pH control. *Water Res.* **1997**, *31*, 339–342. [CrossRef]
15. Coey, J.M.D.; Cass, S. Magnetic water treatment. *J. Magn. Magn. Mater.* **2000**, *209*, 71–74. [CrossRef]
16. Zuo, Y.; Sun, Y.; Yang, W.; Zhang, K.; Chen, Y.; Yin, X.; Liu, Y. Performance and mechanism of 1-hydroxy ethylidene-1, 1-diphosphonic acid and 2-phosphonobutane-1, 2, 4-tricarboxylic acid in the inhibition of calcium carbonate scale. *J. Mol. Liq.* **2021**, *334*, 116093. [CrossRef]
17. Ji, Y.; Chen, Y.; Le, J.; Qian, M.; Huan, Y.; Yang, W.; Yin, X.; Liu, Y.; Wang, X.; Chen, Y. Highly effective scale inhibition performance of amino trimethylenephosphonic acid on calcium carbonate. *Desalination* **2017**, *422*, 165–173. [CrossRef]
18. Yi, X.; Yang, W.; Tang, Y.; Liu, Y.; Zhou, C. Changes in critical supersaturation in the scaling behavior of calcium carbonate. *Petrochem. Ind.* **2007**, *5*, 467–471.
19. Rayane, M.; Samira, G.; Mohamed, T. Calcium carbonate inhibition by green inhibitors: Thiamine and Pyridoxine. *Desalination* **2017**, *404*, 147–154.
20. Xiong, G.; Kunhuan, H.; Baosong, Q.; Qin, D.; Laixian, L.; Yun, W. The effect of glycine on the growth of calcium carbonate in alkaline silica gel. *J. Cryst. Growth* **2017**, *458*, 60–65.
21. Xia, M.; Lei, W.; Dai, L.; Chu, Y.; Wang, F. Study on the scale inhibition mechanism of phosphine based scale inhibitors on calcium carbonate. *Acta Chim. Sin.* **2010**, *68*, 143–148.
22. Zineb, B.; Jean, G.; Laid, M.; Bruno, S.; Bernard, T. Inhibition of calcium carbonate precipitation by aqueous extract of Paronychia argentea. *J. Cryst. Growth* **2014**, *386*, 208–214.

23. Li, H.; Wu, X.; Liu, Z.; Hu, X. Synergistic scale inhibition performance of green scale inhibitor itaconic acid homopolymer and high-voltage electrostatic field. *Chem. Ind. Eng. Prog.* **2009**, *28*, 233–234.
24. Liu, Z.; Zhao, J.; Zhao, J.; Long, S.; Xia, T.; Zhang, X.; An, H. Analysis of Electric Field Distribution and Scale Inhibition Effect in High Voltage Electrostatic Water Treatment Unit. *Proceeding CSEE* **2014**, *34*, 6296–6303.
25. Wu, X.; Liu, Z.; Li, H.; Hu, X. Study on the synergistic scale inhibition effect of itaconic acid homopolymer and high-voltage electrostatic field. *Ind. Water Treat.* **2010**, *30*, 33–35.
26. Liu, Z.; Wang, Y.; Zhao, J.; An, H.; Yang, X.; Zhao, X.; Gao, X. Analysis of Scale Inhibition Effect of Uniform and Non Uniform Electrostatic Fields on Circulating Cooling Water in Industrial Water Treatment. *Ind. Water Treat.* **2018**, *38*, 28–30+34.
27. Chen, Y.; Chen, X.; Zhang, X.; Liu, S.; Wang, C. Anti crystallization test of tunnel permanent magnet drainage pipe based on magnetic processing method. *Tunn. Constr.* **2022**, *42*, 2105–2111.
28. Liu, S. Research on the Mechanism of Flocking and Anti Crystallization Blockage in Tunnel Drainage Pipes. Ph.D. Thesis, Chongqing Jiaotong University, Chongqing, China, 2021.
29. Zhang, X.; Liu, S.; Gao, F.; Zhou, Y.; Zhang, B. Anti Crystallization Blocking of Flocking Drainage Pipe Based on Natural Phenomenon. *Mater. Sci.* **2022**, *28*, 457–466. [CrossRef]
30. Mangestiyono, W.; Muryanto, S.; Jamari, J.; Bayuseno, A.P. The Influence of Vibration on $CaCO_3$ Scale Formation in Piping System. In *MATEC Web of Conferences*; EDP Sciences: Paris, France, 2016; Volume 58, p. 01027.
31. Mangestiyono, W.; Muryanto, S.; Jamari, J.; Bayuseno, A.P. Mitigation of $CaCO_3$ scale formation in pipes under influence of vibration additives Rasayan. *J. Chem.* **2019**, *12*, 192–204.
32. Xiao, J.; Luo, Y.; Yao, Q.; Wu, J.; Lyu, S.; Luo, Z. A self-cleaning coating on copper for inhibiting calcium carbonate crystallization and scaling. *Surf. Coat. Technol.* **2024**, *489*, 131056. [CrossRef]
33. Abdel-Aal, N.; Sawada, K. Inhibition of adhesion and precipitation of $CaCO_3$ by aminopolyphosphonate. *J. Cryst. Growth* **2003**, *256*, 188–200. [CrossRef]
34. Raj, R.; Morozov, Y.; Calado, L.M.; Taryba, M.G.; Kahraman, R.; Shakoor, A.; Montemor, M.F. Inhibitor loaded calcium carbonate microparticles for corrosion protection of epoxy-coated carbon steel. *Electrochim. Acta* **2019**, *319*, 801–812.
35. MacAdam, J.; Parsons, S.A. Calcium carbonate scale formation and control. *Re/Views Environ. Sci. Bio/Technol.* **2004**, *3*, 159–169. [CrossRef]
36. Xu, J.; Zhao, J.; Jia, Y. Experimental study on the scale inhibition effect of the alternating electromagnetic field on $CaCO_3$ fouling on the heat exchanger surface in different circulating cooling water conditions. *Int. J. Therm. Sci.* **2023**, *192*, 108388. [CrossRef]
37. Liu, B.; Guo, X.; Li, Q.; Jia, W.; Sun, H. Effect of Sweep Frequency Electromagnetic Field on $CaCO_3$ Scale Formation in Industrial Circulating Water. *Pol. J. Environ. Stud.* **2023**, *32*, 145–153. [CrossRef] [PubMed]
38. Wang, J.; Zhang, J.; Liang, Y.; Xu, Y. Application of excitation current to characterize the state of calcium carbonate fouling on heat transfer surface under alternating magnetic field. *Int. J. Heat Mass Transf.* **2024**, *224*, 125304. [CrossRef]
39. Lv, C.; Tang, C.-S.; Zhang, J.-Z.; Liu, H.; Pan, X.-H. Regulating the process of microbially induced calcium carbonate precipitation through applied electric fields: Evidence and insights using microfluidics. *J. Geotech. Geoenviron. Eng.* **2024**, *150*, 04024087. [CrossRef]